HHS Public Access

Author manuscript

Ultrasound Med Biol. Author manuscript; available in PMC 2022 May 01.

Published in final edited form as:

Ultrasound Med Biol. 2021 May ; 47(5): 1356–1366. doi:10.1016/j.ultrasmedbio.2021.01.025.

Transcranial Focused Ultrasound Enhances Sensory Discrimination Capability through Somatosensory Cortical Excitation

Chang Liu[†,#], **Kai Yu**[†], **Xiaodan Niu**, **Bin He**[*]

Department of Biomedical Engineering, Carnegie Mellon University

Abstract

Low-intensity transcranial focused ultrasound (tFUS) has emerged as a non-invasive brain neuromodulation tool with high spatial specificity. Previous studies inferred that the tFUS-enhanced sensory performances were attributed to the ultrasound-induced inhibitory neural effects. However, to date there is no direct evidence validating the neural mechanism behind the ultrasound-mediated somatosensory enhancement. In this study, healthy human subjects (N = 9) were asked to perform tactile vibration frequency discrimination tasks while tFUS was directed onto the primary somatosensory cortex. During this task, we simultaneously recorded 64-channel electroencephalogram (EEG) and investigated the brain responses at both EEG sensors and source domains by means of electrophysiological source imaging (ESI). The behavioral results showed that the subjects' vibration frequency discrimination ability was improved by tFUS with an increased percentage of response correct. EEG and ESI results revealed that tFUS neuromodulation was able to improve the sensory discrimination capability through excitatory effects at the targeted sensory cortex.

Keywords

Transcranial focused ultrasound; Neuromodulation; Sensory discrimination; Somatosensory evoked potential; Electrophysiological source imaging

Introduction

Transcranial focused ultrasound (tFUS) has been developed as a novel non-invasive neuromodulation tool by delivering controlled mechanical energy to the target brain area, modulating region-specific brain circuits and networks with high spatial specificity (Tufail et al. 2010, Legon et al. 2014, Lee et al. 2016, Dallapiazza et al. 2018, Niu et al. 2018, Folloni et al. 2019, Kubanek et al. 2020). Pilot studies have investigated the neural effects of tFUS at

[*]Correspondence: Bin He, PhD, Department of Biomedical Engineering, Carnegie Mellon University, 5000 Forbes Avenue, Pittsburgh, PA 15213, USA, bhe1@andrew.cmu.edu, Phone: (412) 268-9857.

[†]These authors contributed equally to this work.

[#]Present address: Boston University, Boston, MA 02215, USA

cortical regions of healthy humans, including primary somatosensory (Legon et al. 2014, Lee et al. 2015, Lee et al. 2016), motor (Gibson et al. 2018, Legon et al. 2018) and visual cortices (Lee et al. 2016, Schimek et al. 2020), demonstrating its capability of focally modulating the cortical functions. Recently, tFUS was directed to modulate the right prefrontal cortex of healthy human participants, decrease the resting state functional connectivity at the emotional regulation cortical networks and increase self-reported global affect (Sanguinetti et al. 2020). The transcranial ultrasound (TUS) was also administered to treat human neural disorders reported by Hameroff et al., in which the posterior frontal cortex was modulated in order to improve mood and reduce chronic pain on patients (Hameroff et al. 2013). A recent study on using ultrasonic thalamic stimulation suggested that this non-invasive brain stimulation tool may assist a patient to recover consciousness after severe brain injury (Monti et al. 2016). Very recently, low-intensity TUS was demonstrated to mitigate worry and increase happiness on a group of college students who suffered from mild to moderate depression through a randomized, double-blind and placebo-controlled study (Reznik et al. 2020).

Among these studies, Legon et al. first demonstrated tFUS to modulate human somatosensory-evoked potential (SEP) elicited by median nerve stimulation through a local inhibitory effect manifested by the decrease of SEP amplitudes. In this pioneering work, they also reported that tFUS improved the human subjects' performances in a tactile frequency discrimination task (Legon et al. 2014). And such a behavioral enhancement was believed to be attributed to the "increased local inhibition" (Legon et al. 2014) or "effective neuronal inhibition" (Legon et al. 2018) conferred by the low-intensity tFUS. However, no concurrent brain recording evidence was presented so far to confirm the hypothetical inhibitory process or directly address a more fundamental question on how the low-intensity tFUS interacting with the targeted somatosensory circuits specifically in processing the sensory discrimination task, thus provide an evidence-based reason of why tFUS leading to the sensory performance advantage.

In this study, we improve upon the experimental design of vibration frequency discrimination task by introducing balanced frequency changes, i.e. increased/decreased/maintained tactile frequencies, when target the tFUS stimulation at the primary somatosensory cortex (S1). 64-channel EEG is recorded simultaneously during the behavior task and brain electrophysiological responses are investigated at both sensor and source domains using the electrophysiological source imaging (ESI) (Yu et al. 2016, Niu et al. 2018, Yu et al. 2020) to investigate the effect of tFUS stimulation on the brain activities during the sensory discrimination task. The results show that tFUS stimulation can enhance the sensory discrimination capability with a higher percentage of response correct (PRC) through excitatory neuromodulation at the sensory cortical areas.

Materials and Methods

Participants

Nine healthy participants were recruited in this experiment (4 females and 5 males, mean age of all participants: 35.77±14.06 years). The study was reviewed and approved by the Institutional Review Board at Carnegie Mellon University. Informed consent was obtained

from all human subjects in accordance with the WORLD Medical Association Declaration of Helsinki.

Experimental Setup

Before the EEG-tFUS experiment, each participant participated a 3-T magnetic resonance imaging (MAGNETOM Verio, Siemens, Malvern, PA, USA) scanning to obtain magnetization-prepared rapid gradient-echo (MP-RAGE) T1-weighted brain structural images. The structural MRI was collected in order to establish individualized brain anatomical model, thus helping identify the brain target through FreeSurfer software (FreeSurfer 6.0, Athinoula A. Martinos Center for Biomedical Imaging, Charlestown, MA, USA) for topological and geometrical segmented brain surfaces (Dale et al. 1999, Desikan et al. 2006), thus guiding the low-intensity focused ultrasound energy onto the subject-specific primary finger sensory cortical region based on a finger sensation map (Penfield and Boldrey 1937).

Each participant attended a sensory task in which computer-programmed mechanical vibrations were delivered to a flat metal plate held between the thumb and index fingers of the right hand when seated in a sound and electromagnetic shielding booth (Customized model, IAC Acoustics, North Aurora, IL, USA). 64-channel electroencephalography (EEG) data were simultaneously acquired by BrainAmp (Brain Products GmbH, Gilching, Germany), with FCz and AFz set as reference and ground electrodes, respectively. The impedances of all electrodes were reduced to be below 10 kΩ by applying a high-chloride, abrasive electrolyte gel (ABRALYT HiCl, EASYCAP GmbH, Herrsching, Germany) before recording. The EEG signals were sampled at 5 kHz. Positions of electrodes were digitized over each subjects' scalp using EEG PinPoint system (Localite GmbH, Bonn, Germany). The ultrasound transducer was mounted over the EEG cap by a 3D-printed helmet. An optical-based brain navigation system (TMS Navigator, Localite GmbH, Bonn, Germany) was employed with the input of the structural MRI data and optical markers attached on the forehead to track the position and orientation of the ultrasound transducer in real time.

Experiment Procedures

The overall experiment setup and procedure is shown in Figure 1. The sensory task was repeated in two different sessions, i.e. Sham US and UPRF 300Hz. In each session, subjects were presented with a pair of vibration stimuli with different frequencies (i.e. f1 and f2) and respective visual cues in each of total 56 trials. In each trial, they were instructed to select the one with a higher vibrating frequency by pressing a corresponding button. The pair of vibration stimuli consisted of one vibration frequency (i.e. f1) fixed at 130 Hz and another frequency centered at 130 Hz with a randomized frequency shift among 7 different levels: 0, 4, 8, 12, 16, 20, 24 Hz, with equal probability to increase or decrease. Each vibration lasted for 1.9 seconds. For each shifted frequency level, 4 trials with increasing shifted frequency and 4 trials with decreasing shifted frequency were presented in one session. The order of these trials was randomized. The mechanical vibrations were delivered to the subject through a flat plate (PHUA8060-35A-33-000, TDK Corp., Tokyo, Japan) held between the thumb and index finger of the right hand. The amplitude at each vibration frequency among the overall range of 106 to 154 Hz was normalized using a force sensor (TN1012/ST

Transducer, ADInstruments Inc., Dunedin, New Zealand). The vibrational frequencies were generated and played from a computer program and were further converted to the mechanical vibration on the plate through a driving board (DRV2667EVM-CT, Texas Instruments, Inc., Dallas, TX, USA). The possible audible sounds produced by the gentle vibration of the plate is further minimized by applying ear plugs (Figure 1).

During the session, the visual cues were displayed on a 24-inch LCD monitor with a viewing distance of 50 cm. Two blocks on the screen with the digit “1” and “2” inside indicated the first and the second vibration in one trial. When the vibration was presented, the corresponding block was highlighted and turned red as a visual cue. After two vibrations presented, each subject had 2 seconds to decide and select the one with a higher vibrating frequency. The entire keyboard was divided and labeled as two parts, i.e. 1 or 2, and the subject was able to press any key in the corresponding side using the left hand to report the selection, which minimized the motion of selection. As visual feedback and confirmation, the background of the corresponding block on the screen turned to gray after the selection was reported. The subject was allowed to skip without pressing any button if they considered the two vibrating frequencies were equal. The subject can change their selection during the decision period. After the decision period, the subject had 1 second of rest interval before the start of the next trial. Their selections during all trials were recorded and saved after the completion of the entire session.

As illustrated in the experimental event sequence (the bottom panel of Figure 1), pulsed ultrasound stimulations were delivered to the finger representation area of S1 at 100 ms before the onset of each vibration stimulus to the fingers. Each sonication lasted for 500 ms with an ultrasound pulse repetition frequency (UPRF) of 300 Hz practiced in the session (denoted as “UPRF 300Hz” condition). In addition, a sham ultrasound session was also conducted with active acoustic transmission, but the ultrasound is physically decoupled to the scalp by 4–6 centimeters (denoted as “Sham US” condition). The sham condition with active acoustic transmission controls for confounding factors such as audible sound generated from the UPRF and electromagnetic interference. The order of the sessions/conditions was also randomized when presented to the human subject. The control of event sequences, such as the timing of vibration stimuli, ultrasound triggering, and the visual interface were programmed in Python (Version 3.7.1, Python Software Foundation, Wilmington, DE, USA) with Psychopy (Version 3.0.4, University of Nottingham, Nottingham, UK)

Ultrasound Setup

A single element focused transducer (AT31529, Blatek Industries, Inc., State College, PA, USA) with an element diameter of 25.4 mm and a focal length of 38.1 mm was used in this study. A 3D-printed collimator (an outlet diameter of 18 mm and a height of 20 mm) filled with ultrasound transmission gel (Aquasonic 100, Parker Laboratories, Inc., Fairfield, NJ, USA) was attached to the transducer for an improved coupling of ultrasound to the scalp. The focused ultrasound wave was generated by the ultrasound transducer, which was driven by two function generators (33220A, Keysight Technologies, Inc., Santa Rosa, CA, USA) and subsequently a radiofrequency (RF) power amplifier (2100L, Electronics & Innovation,

Ltd., Rochester, NY, USA). The first function generator, synchronized by a TTL (transistor-transistor logic) signal from the computer to trigger ultrasound pulses, thus generating the specified number of pulses at the UPRF of 300 Hz. The second function generator, triggered by the output of the first one in a burst mode, was employed to engender ultrasound fundamental frequency (UFF) and determine the cycles per pulse (CPP) number. The ultrasound temporal profile is depicted in Figure 2A.

In this study, the ultrasound setup used a UFF of 0.5 MHz, CPP number of 100. Each sonication lasted for 500 ms with a UPRF of 300 Hz. The spatial peak ultrasound pressure applied to the scalp was measured as 780.4 kPa (Figure 2B–C, spatial-peak pulse-average intensity I_{SPPA}: 5.64 W/cm^2, spatial-peak temporal-average intensity I_{SPTA}: 338.28 mW/cm^2), with an estimated ultrasound pressure of 286.0 kPa (I_{SPPA}: 1.10 W/cm^2, I_{SPTA}: 67.13 mW/cm^2) arriving at the targeted cortical brain. The axial view of the transcranial ultrasound pressure field is presented in Figure 2E, which is also co-registered with an intersectional view as indicated in Figure 2D of a human skull model (Spitzer and Whitlock 1998). This pressure estimation was based on a 3-dimensional transcranial ultrasound scanning using a needle hydrophone (HNR-0500, Onda Corp., Sunnyvale, CA, USA) in the presence of a real human hydrated skull sample (OK-14472, Skulls Unlimited International, Inc., Oklahoma City, OK, USA).

Behavior Data Analysis

For each session, the order of the actual vibration frequencies was saved and converted to a list of indexes of the higher frequency in each trial. The subject's selections during the experiment were also saved and compared with the ground truth to calculate the percentage of responses correct (PRC) for each shifted frequency level (7 PRC measurements for each session). A two-way analysis of variance (ANOVA) test is conducted on PRC data of all subjects to examine the effect of shifted frequency levels and ultrasound conditions. PRCs were then averaged across shifted frequency levels, sessions and subjects. Error bars in standard deviations were plotted for the behavioral data visualization. The statistics of the PRC averaged across all shifted frequency levels in UPRF 300Hz sessions in comparison with those in Sham US were assessed by a one-tail paired Wilcoxon signed rank test with a null hypothesis that the PRC in the UPRF 300Hz session was no greater than that in the Sham US session. This analysis was performed in Matlab (R2019a, Mathworks, Natick, MA, USA) and Python (Version 3.7.1, Python Software Foundation, Wilmington, DE, USA).

Electrophysiological Signal Processing and Analyses

EEG data were band-pass-filtered from 1 to 45 Hz with an infinite impulse response (IIR) filter. Independent component analysis (ICA) was performed to remove components related to eye movements. Data trials were extracted from 0 to 600 ms, while data from −400 to 0 ms were used as baseline and removed after normalization (time 0 was the ultrasound onset). Data in each session were averaged over trials to obtain the ultrasound-evoked brain activities. The EEG temporal profiles and the topographic voltage maps of the ultrasound-modulated brain activities were plotted. A non-parametric permutation-based t-test was performed to assess the statistics of the averaged EEG signal from four electrodes closest to

the target brain region in the two experiment conditions. Data were processed and visualized in MATLAB (R2019a, Mathworks, Natick, MA, USA) using Brainstorm toolbox (Tadel et al. 2011).

Individual MRI data, preprocessed by FreeSurfer for structural brain segmentation, was co-registered with the digitization of the EEG electrodes. The individualized head boundary element method (BEM) model (He et al. 1987, Hämäläinen and Sarvas 1989) was further created in Brainstorm for each participant. The averaged ultrasound-modulated somatosensory brain activities in each condition for all participants were processed following the electrophysiological source imaging pipeline (Michel and He 2017, He et al. 2018). The minimum norm imaging (MNI) algorithm was applied to solve the inverse problem and further reconstruct the current source density (CSD) (Dale and Sereno 1993) at the cortical regions of interest (ROI). A finger representation area of 3.8 – 4.2 cm^2 on the primary somatosensory cortex in the left hemisphere was selected as the brain ROI, and the averaged source amplitude, denoted as the sensory source profile amplitude (SSPA), within this ROI was extracted for further statistical analyses (Babiloni et al. 2005, Edelman et al. 2016). A one-tail paired Wilcoxon signed rank test was performed to investigate the statistics of the SSPAs in the two experiment conditions with a null hypothesis that the SSPA in the UPRF 300Hz session was no greater than that in the Sham US session. The SSPA is defined as the difference between the maximum and the minimum of averaged CSD in time. This analysis was also performed in MATLAB (R2019a, Mathworks, Natick, MA, USA) and Python (Version 3.7.1, Python Software Foundation, Wilmington, DE, USA).

Results

Behavior Outcomes

A two-way ANOVA test is conducted on PRC data of all subjects to examine the effect of shifted frequency levels (7 levels) and ultrasound conditions (Sham US and UPRF 300Hz). The result shows that both shifted frequency levels ($F_{6,112} = 2.87$, $p = 0.012$, effect size $\eta_p^2 = 0.13$) and ultrasound conditions ($F_{1,112} = 8.37$, $p = 0.005$, effect size $\eta_p^2 = 0.07$) have statistically significant effects on the PRC, which indicates that tFUS is able to increase the subjects' discrimination ability in sensing the frequencies of mechanical vibrations. No significant interaction between the effect of shifted frequency levels and ultrasound conditions was observed ($F_{6,112} = 0.39$, $p = 0.88$, effect size $\eta_p^2 = 0.02$).

The behavior results are also depicted in Figure 3. Each line in Figure 3A represents the averaged PRC over subjects (N = 9) with respect to different shifted vibration frequency level in each condition. In both conditions, the PRC increases as the shifted frequency increases. As the subjects were asked to skip pushing buttons if the two frequencies were considered equal, three options were provided for each decision and the chance level was 33%. In Sham US, the average PRC across all shifted frequencies was 34.92% and the mean PRCs were above the chance level when the shifted vibration frequencies were greater than 8 Hz. In UPRF 300Hz, PRCs were greater than the chance level at all shifted frequency levels, while the overall PRC reached 45.24%. A testing threshold, which was defined as the minimum shifted frequency while the PRC reached 50%, became lower in UPRF 300Hz condition than that in Sham US. A one-tail paired Wilcoxon test was also implemented to

examine the null hypothesis that the PRC in UPRF 300Hz condition would be no greater than that in Sham US condition. As a result, it showed significant improvements ($p = 0.048$, effect size $r = 0.39$) of subjects' median PRC during UPRF 300Hz in comparison with those in the Sham US condition, shown in Figure 3B. These data demonstrate that ultrasound increases the overall PRC compared with the sham condition, which support the previous experimental finding (Legon et al. 2014).

EEG Responses at the Sensor Domain

The averaged 64-channel EEG sensor-level result across multiple subjects (N = 7) is shown as butterfly plots in Figure 4A and B. Due to relatively severe body movements during the task, two subjects with poor EEG signal quality were excluded for further data analyses. The vibrational sensory-evoked brain activities in Sham US and UPRF 300Hz conditions are depicted.

The averaged EEG signal of C3, C5, CP3, CP5 (N = 7) in solid lines, which are the four electrodes closest to the brain region of the ultrasound neuromodulation, is shown in Figure 4C. The shaded areas under the solid lines represent the standard error of the mean (S.E.M.), and gray vertical bars indicate those temporal segments in the UPRF 300Hz condition which are significantly different from the signal in Sham US condition ($p < 0.05$, non-parametric permutation-based t-test). Compared with the Sham US condition, N30, P100-N170 components are significantly enhanced with the neuromodulation in UPRF 300Hz. The existent N300 component in Sham US condition is also modulated in the UPRF 300Hz condition which shows statistically significant differences when comparing to the tFUS condition.

Topographic maps of the averaged EEG signal, under each condition at 30 ms, 100 ms and 330 ms when the statistical significance is shown, are presented in Figure 4D–I. The topo maps are displayed in the grand average reference montage. At 30 ms and 100 ms, the topo maps of UPRF 300Hz condition show different spatial patterns (Figure 4G and H) with stronger activations in frontal and temporal lobes than those of Sham US. At 330 ms, the topo map in UPRF 300Hz condition presents a similar spatial pattern as in the Sham US but with a stronger magnitude.

EEG Responses at the Source Domain

Figure 5A–D show the electrophysiological source imaging result at 100 and 330 ms under Sham US and UPRF 300Hz conditions. At 100 ms, there is no significant brain activation (maximum CSD of 15.5 pA·m, Figure 5A) on the S1 in the Sham US condition, whereas the activation appears at the S1 in UPRF 300Hz condition with the maximum CSD of 565.1 pA·m (Figure 5B). At 300–400 ms, the S1 activation with maximum CSD of 92.9 pA·m exists in Sham US condition (Figure 5C), and more sensory cortical activations are localized in the UPRF 300Hz condition with a higher CSD maximum value of 576.7 pA·m (Figure 5D).

The green patches in the Figure 5A–D are used to identify the ROI in this study, i.e. the finger representation area on the S1 in the left hemisphere. The averaged CSD (N = 7) of this ROI in each condition is extracted from the identified area of 4 cm^2 and presented in

Figure 5E. The grand averaged CSD is depicted with solid line profiles, and the shaded areas indicate the S.E.M. In the early SEP source complex during 90–110 ms, the grand averaged SSPA is 51.7 pA·m in UPRF 300Hz condition comparing to the much less mean amplitude of 5.0 pA.m in Sham US. In the late SEP source complex during 300–400 ms, the absolute value of SSPA is increased from 13.4 in Sham US condition to 31.0 pA·m in UPRF 300Hz. Furthermore, as illustrated in Figure 5F, the SSPA is significantly increased in the UPRF 300Hz condition compared with that in the Sham US, examined by a one-tail paired Wilcoxon signed rank test ($p = 0.026$, effect size $r = 0.51$).

Discussion

In this study, we performed a mechanical vibration frequency discrimination task in a group of healthy human subjects and evaluated the performance of participants under the low-intensity tFUS neuromodulation condition with a UPRF of 300 Hz and the sham condition. In both conditions, the behavior results show a tendency that the percentage of responses correct (PRC) increased as the shifted frequency increased, which aligns the intuition that it is easier for subjects to differentiate two frequencies once the frequency difference becomes larger. The behavior results also illustrated that subjects exhibited a higher overall PRC when their central sensory brain circuits were modulated with tFUS in comparison with the sham condition. These results revealed that low-intensity tFUS stimulation at the S1 may improve the vibration frequency discrimination capability, which was consistent with the behavioral results in the previous work (Legon et al. 2014).

Given the behavior outcome, a fundamental question remains that whether the frequency discrimination enhancement is due to the inhibitory or excitatory neuromodulation effects of tFUS. To directly address this question, we simultaneously recorded multi-channel EEG to objectively assess the brain responses to the sensory input and performed analyses on concurrent EEG data at the sensor and source domains to uncover electrophysiological evidence. In the sham condition, a negative peak occurred 200 ms after the onset of the vibration stimuli which corresponded to the N300 component in the temporal signal (vibration stimuli were presented 100 ms after ultrasound onsets). The cortical source amplitude of this component indicated that the finger representation areas at the primary somatosensory cortex was activated during the task. When tFUS was delivered to S1, a significant difference from the sham condition showed that the magnitude of the N300 component became enhanced at the sensor level (Figure 3C). The reconstructed source results also showed that the activation on S1 demonstrated a higher source profile amplitude. The early phase (e.g. < 150 ms) of the SEP enhancement is deemed to be associated with excitatory effects on the afferent vibrotactile signal transmission and brain processing at the specific primary somatosensory cortex (S1) (Schubert et al. 2006). The increased excitability (Gibson et al. 2018, Yu et al. 2020) of the S1 due to the ultrasound modulation may be responsible to such excitatory effects, which does not exclude the possible ultrasound-evoked potential (Lee et al. 2015, Yu et al. 2016) in addition to the SEP at S1. The late phase (e.g. > 200 ms) of the enhanced SEP may be related to the increased associative cortical reactions for the secondary somatosensory information processing occurring at the adjacent brain circuits. The increased S1 activities may provide enhanced communications to the associative brain network. These results revealed that tFUS stimulation targeting the

activated brain area in the sensory task may increase the local brain excitability, thus leading to the enhancement of sensory discrimination capability.

It was suggested that such enhancement of sensory discrimination capability was attributed to effective neuronal inhibition by the administered tFUS (Legon et al. 2014, Legon et al. 2018). However, such neuronal inhibitory effect was observed from tFUS-mediated median nerve stimulation paradigm, and no concurrent EEG was recorded to directly support the same neural mechanism. To explain such a difference between our observations in the present work and the previous experiment outcomes, the UPRF may play a significant role (King et al. 2013, Plaksin et al. 2016, Kubanek et al. 2018, Yu et al. 2019) in changing the results. We applied relatively low UPRF (i.e. 300 Hz) to the human primary somatosensory cortex comparing to the 1 kHz UPRF employed by Legon et al. (Legon et al. 2014, Legon et al. 2018). Moreover, the UPRF employed in our work is even lower than that was applied by Lee et al. (Lee et al. 2015), in which the excitatory neural effects of tFUS (UPRF = 500 Hz) were reported at the human S1 cortical region. By further tuning the tFUS parameters, such as the UPRF, may shed light on the parameter-dependent neuromodulation effects of tFUS in humans. Besides the ultrasound parameters, the neuromodulation effect of tFUS may also depend on the state of brain circuits, such that the closed-loop transcranial ultrasound has been shown to deliver timely and effective neuromodulation according to the state of brain activities in *in vivo* rodent models (Yang et al. 2020). In other words, the brain states might be different in median nerve stimulation paradigm versus frequency discrimination task, thus the tFUS neuromodulation leading to inhibitory versus excitatory effects in S1. Nevertheless, elucidating the potential roles of these factors for tFUS in generating excitatory/inhibitory neuromodulatory effects at the somatosensory circuits is of great importance for effective translational applications of ultrasound neuromodulation on human, such as managing chronic neuropathic pain (Yu et al. 2020) in which the somatosensory cortices will be considered as essential brain targets for neuromodulation, as they are deemed as important circuits associated with nociception and processing the sensory aspect of the pain (Case et al. 2017).

The tFUS employed in our study is generally safe and no adverse effect was reported by the human subjects through brief surveys of possible symptoms, such as headache, nausea, and dizziness, etc. To ensure the safety, we limited the tFUS intensities lower than the FDA safety guidelines for diagnostic ultrasound (FDA 2019), as well as the ultrasound intensities administered by Legon et al. (Legon et al. 2014, Legon et al. 2020).

For a rigorous investigation, our experiments introduced the sham ultrasound session with active ultrasound transmission while detached the acoustic aperture from the scalp. As the transducer did not directly touch the scalp in both ultrasound sessions and the ultrasound transmission gel still covered the subject’s scalp at the target area in the Sham US setup, it would be a very similar sensory perception by the subjects. During the experiment, the transducer was held by a clamp which was mounted on the plastic helmet; thus, the same weight/pressure was applied to the subject’s scalp in both actual and sham ultrasound conditions. Therefore, the subjects felt the ultrasound transmission gel all the time throughout the testing sessions and would feel no difference in terms of the scalp sensations. Furthermore, although the order of the two sessions with different ultrasound settings was

randomized to our capacity, some confounding factors in the experiment design may still bias the behavioral outcome. As the sessions were scheduled in one day with short breaks in between, the subject may have better performance in the latter session because of a potential learning effect that the subject became more familiar with the task. On the other hand, the subject may experience fatigue in the latter session, thus the performance may become worse due to the fatigue.

It was also observed that the targeted brain region was active at early times (30–40 ms, 90–100 ms) after the tFUS onset (Figure 4A and B). During these two time periods, no vibration stimuli were actually presented yet to the human subjects, which implied that these activations may be directly elicited by tFUS stimulation. Lee et al. also reported similar temporal patterns in 2015 that tFUS elicited evoked potential which was similar to SEP elicited by median nerve stimulation in the hand S1 at electrode sites of C3 and P3 (Lee et al. 2015). However, in our study, the subjects did not report any special awareness/sensation at their fingers during tFUS, while tactile sensations were reported in the previous study. Such differences may result from the difference in ultrasound parameters, including fundamental frequency, pulse repetition frequency, sonication duration and pressure. Furthermore, the external vibration in the concurrent discrimination task may also inevitably distract the subject from the awareness of sensations elicited by tFUS. Nevertheless, the neural effect of tFUS with various parameter sets on directly elicit somatosensory activities at the human brain still merits further investigations so as to better understand the inhibitory/excitatory effects of tFUS stimulation without the presence of any external sensory stimuli.

Acknowledgements

This work was supported in part by NIH grants MH114233, EB029354, AT009263, EB021027, and NS096761. K.Y. was supported in part by The Samuel and Emma Winters Foundation. X.N. was supported in part by Carnegie Mellon Neuroscience Institute Presidential Fellowship and Liang Ji Dian Graduate Fellowship at Carnegie Mellon University.

The authors would like to thank Dr. Abbas Sohrabpour and Dr. Haiteng Jiang for useful discussions, Shahriar Noroozizadeh, Emily Lopez, Xiyuan Jiang and Sandhya Ramachandran for experimental assistance. The authors would also thank the technical support from the CMU-Pitt Brain Imaging Data Generation & Education (BRIDGE) Center for providing the MRI facilities and services.

References

Babiloni F, Cincotti F, Babiloni C, Carducci F, Mattia D, Astolfi L, Basilisco A, Rossini PM, Ding L, Ni Y, Cheng J, Christine K, Sweeney J and He B Estimation of the cortical functional connectivity with the multimodal integration of high-resolution EEG and fMRI data by directed transfer function. Neuroimage 2005;24:118–131. [PubMed: 15588603]

Case M, Zhang H, Mundahl J, Datta Y, Nelson S, Gupta K and He B Characterization of functional brain activity and connectivity using EEG and fMRI in patients with sickle cell disease. NeuroImage: Clinical 2017;14:1–17. [PubMed: 28116239]

Dale AM, Fischl B and Sereno MI Cortical surface-based analysis. I. Segmentation and surface reconstruction. Neuroimage 1999;9:179–194. [PubMed: 9931268]

Dale AM and Sereno MI Improved localization of cortical activity by combining EEG and MEG with MRI cortical surface reconstruction: a linear approach. J. Cognitive Neuroscience 1993;5:162–176.

Dallapiazza RF, Timbie KF, Holmberg S, Gatesman J, Lopes MB, Price RJ, Miller GW and Elias WJ Noninvasive neuromodulation and thalamic mapping with low-intensity focused ultrasound. J Neurosurg 2018;128:875–884. [PubMed: 28430035]

Desikan RS, Segonne F, Fischl B, Quinn BT, Dickerson BC, Blacker D, Buckner RL, Dale AM, Maguire RP, Hyman BT, Albert MS and Killiany RJ An automated labeling system for subdividing the human cerebral cortex on MRI scans into gyral based regions of interest. Neuroimage 2006;31:968–980. [PubMed: 16530430]

Edelman BJ, Baxter B and He B EEG Source Imaging Enhances the Decoding of Complex Right-Hand Motor Imagery Tasks. IEEE Trans Biomed Eng 2016;63:4–14. [PubMed: 26276986]

FDA US Marketing Clearance of Diagnostic Ultrasound Systems and Transducers. U. S. D. H. a. H. Services Rockville, MD, Center for Devices and Radiological Health. 2019.

Folloni D, Verhagen L, Mars RB, Fouragnan E, Constans C, Aubry J-F, Rushworth MFS and Sallet J Manipulation of Subcortical and Deep Cortical Activity in the Primate Brain Using Transcranial Focused Ultrasound Stimulation. Neuron 2019;101:1109–1116.e1105. [PubMed: 30765166]

Gibson BC, Sanguinetti JL, Badran BW, Yu AB, Klein EP, Abbott CC, Hansberger JT and Clark VP Increased Excitability Induced in the Primary Motor Cortex by Transcranial Ultrasound Stimulation. Front Neurol 2018;9:1007. [PubMed: 30546342]

Hämäläinen MS and Sarvas J Realistic conductivity geometry model of the human head for interpretation of neuromagnetic data. IEEE Trans Biomed Eng 1989;36:165–171. [PubMed: 2917762]

Hameroff S, Trakas M, Duffield C, Annabi E, Gerace MB, Boyle P, Lucas A, Amos Q, Buadu A and Badal JJ Transcranial ultrasound (TUS) effects on mental states: a pilot study. Brain Stimul 2013;6:409–415. [PubMed: 22664271]

He B, Musha T, Okamoto Y, Homma S, Nakajima Y and Sato T Electric dipole tracing in the brain by means of the boundary element method and its accuracy. IEEE Trans Biomed Eng 1987;34:406–414. [PubMed: 3610187]

He B, Sohrabpour A, Brown E and Liu Z Electrophysiological Source Imaging: A Noninvasive Window to Brain Dynamics. Annu Rev Biomed Eng 2018;20:171–196. [PubMed: 29494213]

King RL, Brown JR, Newsome WT and Pauly KB Effective parameters for ultrasound-induced in vivo neurostimulation. Ultrasound Med Biol 2013;39:312–331. [PubMed: 23219040]

Kubanek J, Brown J, Ye P, Pauly KB, Moore T and Newsome W Remote, brain region-specific control of choice behavior with ultrasonic waves. Science Advances 2020;6:

Kubanek J, Shukla P, Das A, Baccus SA and Goodman MB Ultrasound Elicits Behavioral Responses through Mechanical Effects on Neurons and Ion Channels in a Simple Nervous System. The Journal of Neuroscience 2018;38:3081–3091. [PubMed: 29463641]

Lee W, Chung YA, Jung Y, Song IU and Yoo SS Simultaneous acoustic stimulation of human primary and secondary somatosensory cortices using transcranial focused ultrasound. BMC Neurosci 2016;17:68. [PubMed: 27784293]

Lee W, Kim H, Jung Y, Song IU, Chung YA and Yoo SS Image-guided transcranial focused ultrasound stimulates human primary somatosensory cortex. Sci Rep 2015;5:8743. [PubMed: 25735418]

Lee W, Kim HC, Jung Y, Chung YA, Song IU, Lee JH and Yoo SS Transcranial focused ultrasound stimulation of human primary visual cortex. Sci Rep 2016;6:34026. [PubMed: 27658372]

Legon W, Adams S, Bansal P, Patel PD, Hobbs L, Ai L, Mueller JK, Meekins G and Gillick BT A retrospective qualitative report of symptoms and safety from transcranial focused ultrasound for neuromodulation in humans. Sci Rep 2020;10:5573. [PubMed: 32221350]

Legon W, Bansal P, Tyshynsky R, Ai L and Mueller JK Transcranial focused ultrasound neuromodulation of the human primary motor cortex. Sci Rep 2018;8:10007. [PubMed: 29968768]

Legon W, Sato TF, Opitz A, Mueller J, Barbour A, Williams A and Tyler WJ Transcranial focused ultrasound modulates the activity of primary somatosensory cortex in humans. Nat Neurosci 2014;17:322–329. [PubMed: 24413698]

Michel C and He B EEG Mapping and Source Imaging. Niedermeyer's Electroencephalography: Basic Principles, Clinical Applications, and Related Fields. Schomer D and Lopes da Silva F. Philadelphia: Wolters Kluwer & Lippincott Williams & Wilkins. 2017;

Monti MM, Schnakers C, Korb AS, Bystritsky A and Vespa PM Non-Invasive Ultrasonic Thalamic Stimulation in Disorders of Consciousness after Severe Brain Injury: A First-in-Man Report. Brain Stimul 2016;9:940–941. [PubMed: 27567470]

Niu X, Yu K and He B On the neuromodulatory pathways of the in vivo brain by means of transcranial focused ultrasound. Current Opinion in Biomedical Engineering 2018;8:61–69. [PubMed: 31223668]

Penfield W and Boldrey E Somatic motor and sensory representation in the cerebral cortex of man as studied by electrical stimulation. Brain 1937;60:389–443.

Plaksin M, Kimmel E and Shoham S Cell-Type-Selective Effects of Intramembrane Cavitation as a Unifying Theoretical Framework for Ultrasonic Neuromodulation. eNeuro 2016;3:ENEURO.0136–15.2016.

Reznik SJ, Sanguinetti JL, Tyler WJ, Daft C and Allen JJB A double-blind pilot study of transcranial ultrasound (TUS) as a five-day intervention: TUS mitigates worry among depressed participants. Neurology, Psychiatry and Brain Research 2020;37:60–66.

Sanguinetti JL, Hameroff S, Smith EE, Sato T, Daft CMW, Tyler WJ and Allen JJB Transcranial Focused Ultrasound to the Right Prefrontal Cortex Improves Mood and Alters Functional Connectivity in Humans. Front Hum Neurosci 2020;14:52. [PubMed: 32184714]

Schimek N, Burke-Conte Z, Abernethy J, Schimek M, Burke-Conte C, Bobola M, Stocco A and Mourad PD Repeated Application of Transcranial Diagnostic Ultrasound Towards the Visual Cortex Induced Illusory Visual Percepts in Healthy Participants. Front Hum Neurosci 2020;14:66. [PubMed: 32194387]

Schubert R, Blankenburg F, Lemm S, Villringer A and Curio G Now you feel it--now you don't: ERP correlates of somatosensory awareness. Psychophysiology 2006;43:31–40. [PubMed: 16629683]

Spitzer VM and Whitlock DG The Visible Human Dataset: the anatomical platform for human simulation. Anat Rec 1998;253:49–57. [PubMed: 9605360]

Tadel F, Baillet S, Mosher JC, Pantazis D and Leahy RM Brainstorm: A User-Friendly Application for MEG/EEG Analysis. Computational Intelligence and Neuroscience 2011; DOI: 10.1155/2011/879716.

Tufail Y, Matyushov A, Baldwin N, Tauchmann ML, Georges J, Yoshihiro A, Tillery SIH and Tyler WJ Transcranial Pulsed Ultrasound Stimulates Intact Brain Circuits. Neuron 2010;66:681–694. [PubMed: 20547127]

Yang H, Yuan Y, Wang X and Li X Closed-Loop Transcranial Ultrasound Stimulation for Real-Time Non-invasive Neuromodulation in vivo. Front Neurosci 2020;14:445. [PubMed: 32477055]

Yu K, Liu C, Niu X and He B Transcranial Focused Ultrasound Neuromodulation of Voluntary Movement-related Cortical Activity in Humans. IEEE Transactions on Biomedical Engineering 2020; DOI: 10.1109/TBME.2020.3030892.

Yu K, Niu X and He B Neuromodulation Management of Chronic Neuropathic Pain in the Central Nervous System. Advanced Functional Materials 2020; DOI: 10.1002/adfm.201908999.

Yu K, Niu X, Krook-Magnuson E and He B Intrinsic Cell-type Selectivity and Inter-neuronal Connectivity Alteration by Transcranial Focused Ultrasound. bioRxiv 2019;576066.

Yu K, Sohrabpour A and He B Electrophysiological Source Imaging of Brain Networks Perturbed by Low-Intensity Transcranial Focused Ultrasound. IEEE Trans Biomed Eng 2016;63:1787–1794. [PubMed: 27448335]

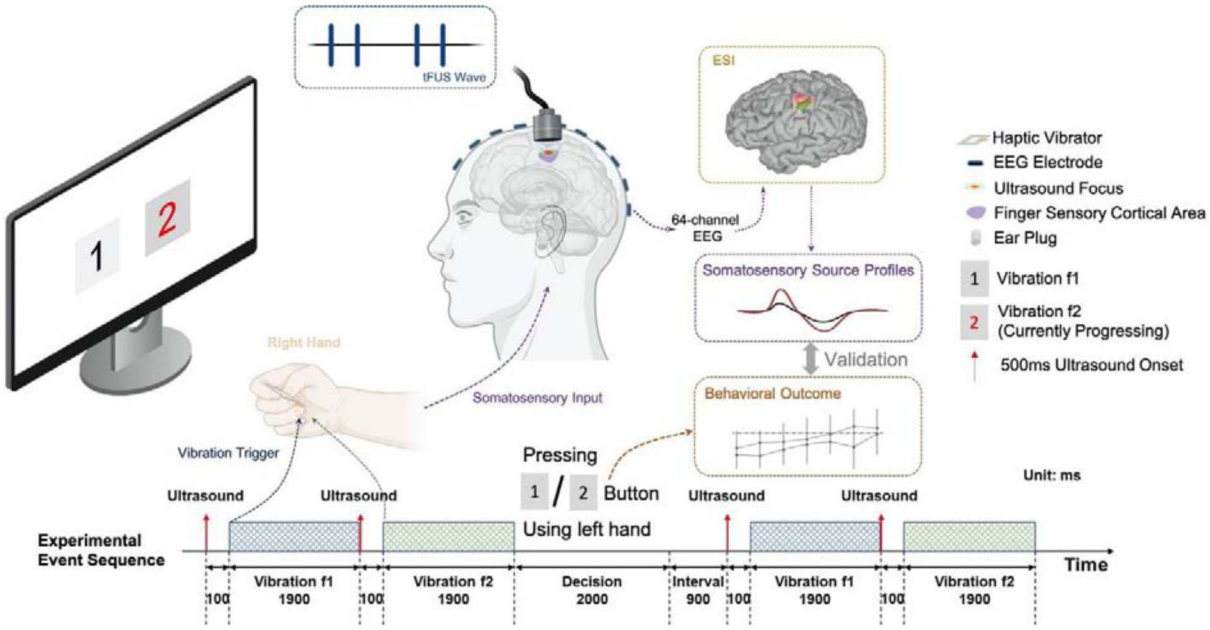

Figure 1.

Diagram of the overall experiment setup and procedure. In each trial, a pair of vibration stimuli are delivered to a flat haptic vibrator held between the subject's thumb and index fingers of the right hand. The subject is instructed to select the one with a higher frequency by pressing corresponding buttons. The status of the stimulus and the decision is shown on the screen in real-time. Transcranial focused ultrasound (tFUS) is delivered to the primary finger somatosensory cortical area at 100 ms before the onset of each vibration stimulus. The 64-channel electroencephalography (EEG) data are simultaneously recorded to perform electrophysiological source imaging (ESI). The reconstructed source activities at the finger somatosensory cortical area are extracted as somatosensory source profiles and are validated with behavior outcomes to further access the tFUS neuromodulation effects.

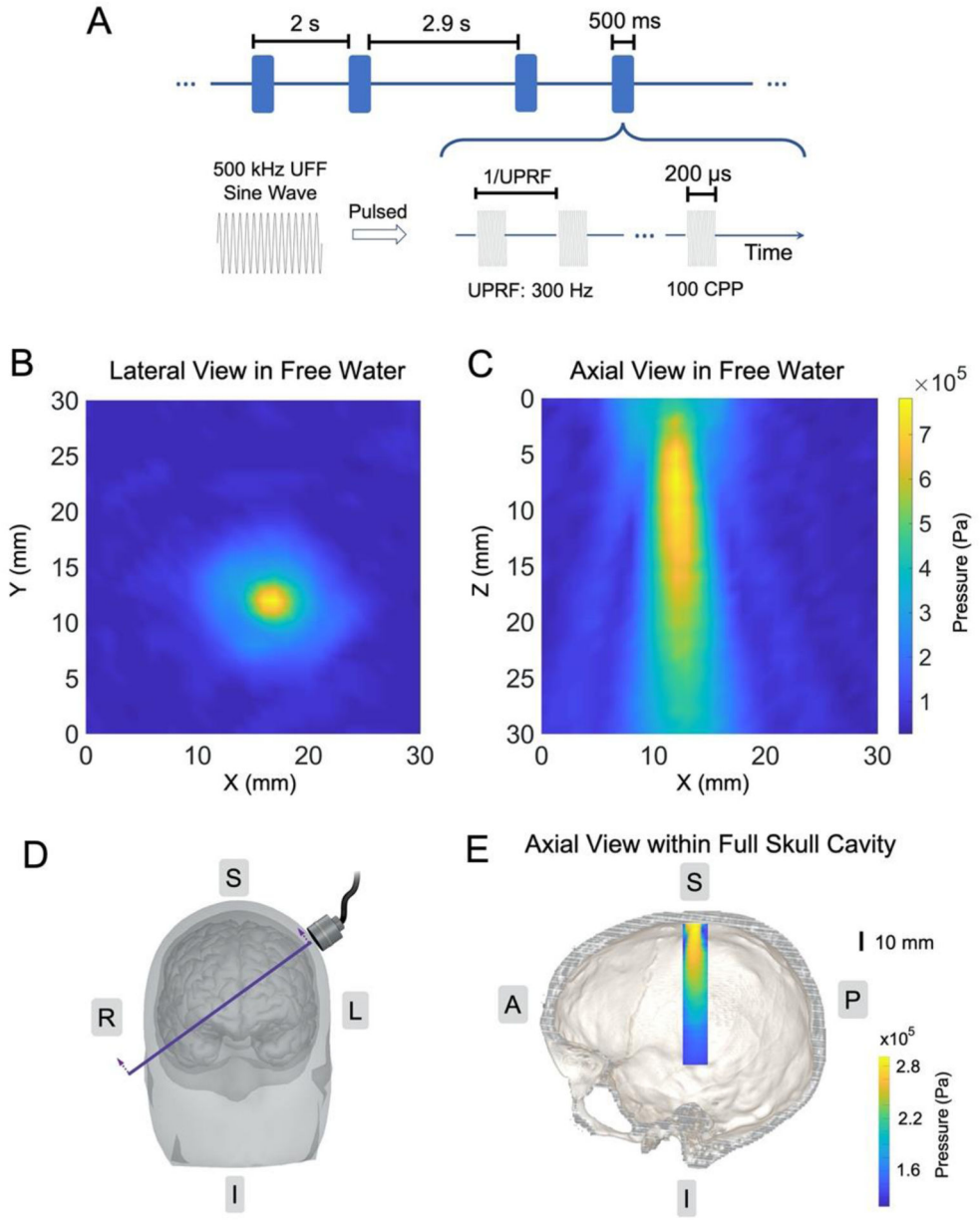

Figure 2.

Ultrasound spatiotemporal profiles. (A) The ultrasound waveform and time sequence. (B-C) Ultrasound pressure field measurements along the lateral direction in free water (B) and along the axial direction in free water (C). (D-E) The illustration of transducer placement over a human head/brain model (D) with the intersectional view of the transcranial ultrasound pressure distribution within a full human skull; the image is co-registered with a human skull model (E).

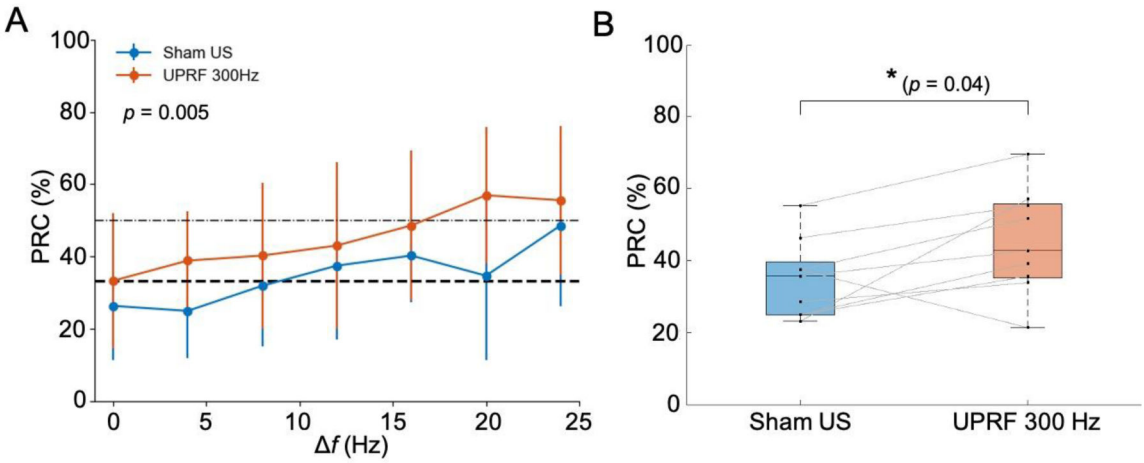

Figure 3.

Behavior outcomes from the frequency discrimination task. (A) The averaged percentage of responses correct (PRC) over subjects (N = 9) with respect to 7 shifted frequency level in each condition. The standard deviations at those 7 frequency levels are indicated with error bars. Ultrasound conditions have a statistically significant effect on the PRC examined by a two-way ANOVA test. (B) The boxplot of the averaged PRC across all shifted frequencies in each ultrasound condition. Statistics by one-tail paired Wilcoxon signed rank test for examining the effect of tFUS increasing the subjects' frequency discrimination accuracy. *$p < 0.05$.

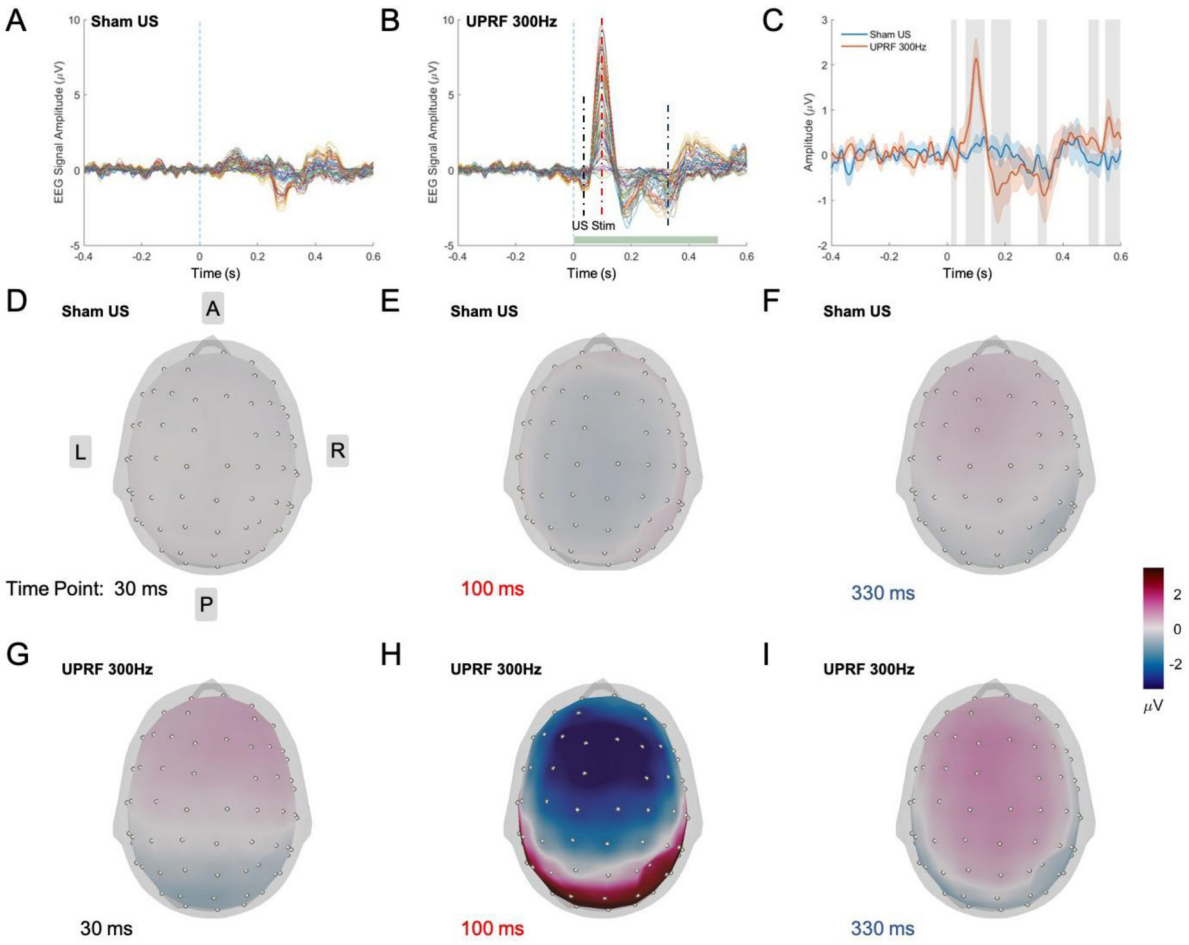

Figure 4.

EEG spatiotemporal responses at the sensor domain. (A-B) The averaged EEG signal over subjects (N = 7) shown in butterfly plots in Sham US (A), and UPRF 300Hz (B) conditions. (C) Averaged EEG signals of electrode C3, C5, CP3, CP5 (N = 7). The solid lines represent the grand averaged EEG signals, and the shaded areas under the solid lines indicate the standard error of the mean (S.E.M.). The vertical gray bars represent the time segments of significant differences between sham and ultrasound conditions. (D-I) Topographic voltage maps of the averaged EEG signal (N = 7) at 30, 100, 330 ms under Sham US (D-F) and UPRF 300Hz (G-I) conditions.

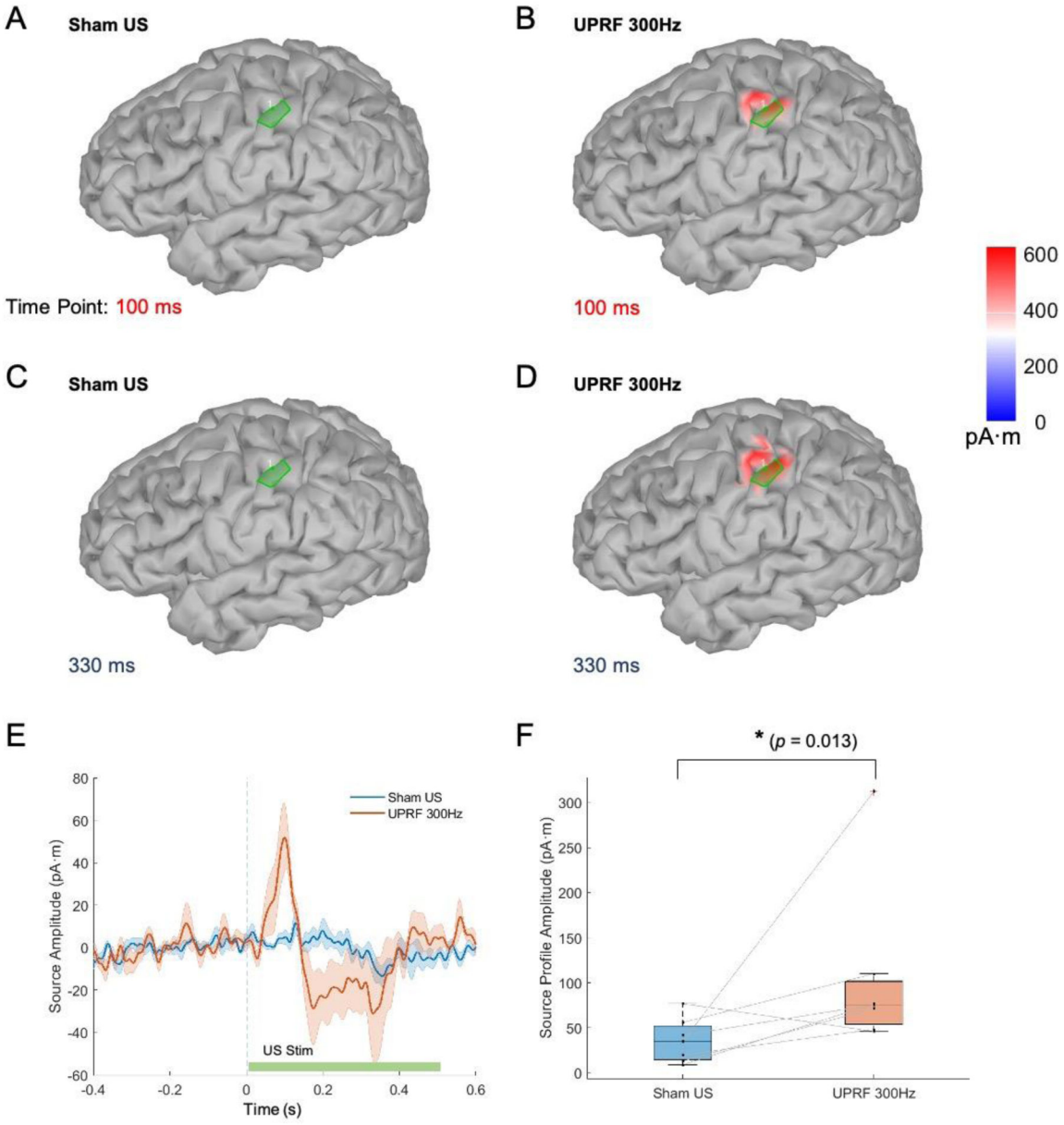

Figure 5.

EEG spatiotemporal responses at the source domain. (A-D) The ESI results (absolute values) at 100 and 330 ms in Sham US (A, C) and UPRF 300Hz (B, D) conditions. (E) The averaged source amplitude (N = 7, solid lines) in the brain region of interest at the left primary somatosensory cortex. The colored and shaded areas behind the solid lines represent the S.E.M. (F) The somatosensory source profile amplitude (SSPA) is significantly increased in the UPRF 300Hz condition compared with that in the Sham US condition, examined by one-tail paired Wilcoxon signed rank test. *$p < 0.05$.